AGU PUBLICATIONS

JGR

Journal of Geophysical Research: Space Physics

RESEARCH ARTICLE
10.1002/2015JA021971

Key Points:
- CADI Doppler drift correlate well with C/NOFS drift and their relation was found to vary with seasons
- Artificial neural network-based approach has been utilized to correct the daytime CADI drift against underestimation
- Corrected CADI EXB drift has also been utilized to model the daytime ionospheric distribution in the SAMI2 model

Correspondence to:
L. M. Joshi,
lmjoshinarl@gmail.com

Citation:
Joshi, L. M., and S. Sripathi (2016), On the utility of the ionosonde Doppler-derived EXB drift during the daytime, *J. Geophys. Res. Space Physics*, *121*, doi:10.1002/2015JA021971.

Received 1 OCT 2015
Accepted 3 MAR 2016
Accepted article online 9 MAR 2016

On the utility of the ionosonde Doppler-derived EXB drift during the daytime

L. M. Joshi[1] and S. Sripathi[1]

[1]Indian Institute of Geomagnetism, Navi Mumbai, India

Abstract Vertical EXB drift measured using the ionosonde Doppler sounding during the daytime suffers from an underestimation of the actual EXB drift because the reflection height of the ionosonde signals is also affected by the photochemistry of the ionosphere. Systematic investigations have indicated a fair/good correlation to exist between the C/NOFS and ionosonde Doppler-measured vertical EXB drift during the daytime over magnetic equator. A detailed analysis, however, indicated that the linear relation between the ionosonde Doppler drift and C/NOFS EXB drift varied with seasons. Thus, solar, seasonal, and also geomagnetic variables were included in the Doppler drift correction, using the artificial neural network-based approach. The RMS error in the neural network was found to be smaller than that in the linear regression analysis. Daytime EXB drift was derived using the neural network which was also used to model the ionospheric redistribution in the SAMI2 model. SAMI2 model reproduced strong (weak) equatorial ionization anomaly (EIA) for cases when neural network corrected daytime vertical EXB drift was high (low). Similar features were also observed in GIM TEC maps. Thus, the results indicate that the neural network can be utilized to derive the vertical EXB drift from its proxies, like the ionosonde Doppler drift. These results indicate that the daytime ionosonde measured vertical EXB drift can be relied upon, provided that adequate corrections are applied to it.

1. Introduction

The equatorial ionization anomaly (EIA) is one of the most comprehensively studied phenomena, pertaining to the equatorial and low latitude ionosphere. It is characterized by plasma density crest region of the ionosphere at 10°–20° dip latitude. It is essentially a daytime phenomenon, when the eastward electric field transports the plasma upward in the EXB direction. The pressure gradient force and the gravitational force cause the plasma to descend along the magnetic field lines and create enhanced plasma density regions at the conjugate low latitudes. The process of the uplift of the plasma due to upward EXB drift and downward diffusion at higher latitudes is commonly referred to as "fountain effect." EIA displays a large day-to-day variability, linked with the variability of zonal electric field and neutral winds. EIA influences the accuracy of the satellite-based navigation, as it alters the ionospheric total electron content (TEC).

The zonal eastward electric field not only creates the plasma fountain but also drives the intense eastward current in the equatorial region, known as equatorial electrojet (EEJ). Based on the geomagnetic observations from the Indian longitude, *Dunford* [1967] revealed a certain relation between the horizontal component of the geomagnetic field and the strength of the EIA. For that investigation, Alouette1 topside sounder was utilized to infer the latitudinal structure of the ionosphere over Indian region. Based on geomagnetic and total electron content (TEC) observations over India, *Deshpande et al.* [1977] found the EIA to be strong on the days with intense EEJ. They found the EIA to be weak on counter electrojet (CEJ) days. Their study also highlighted the response time for the EIA, to the changes in EEJ, to be ~ 2.5 h. *Huang et al.* [1989] found average to good correlation between the EEJ strength and the crest latitude. They also found the correlation coefficients to depend on the seasons of the year, which was attributed to the seasonal variation of the meridional neutral winds. Based on observations from Brazilian longitude, *Abdu et al.* [1990] found a positive correlation between EEJ and the height of the F_2 layer peak in the EIA trough region. They also reported a time lag of about 3 h between the F_2 layer peak height and the enhanced plasma density in the EIA crest. The response of the EIA crest to the EEJ strength was also found to depend on the intensity of the meridional winds. *Rastogi and Klobuchar* [1990] found the EIA crest density to correlate well with the difference in the horizontal magnetic field measured over the magnetic equator and away from the EEJ belt in the low latitude rather than on the horizontal magnetic field measured only at magnetic equator. They utilized the Faraday

rotation measurement on linearly polarized 140 MHz signal from ATS 6 satellite, received over eight different locations, to derive TEC over Indian region. *Su et al*. [1995] utilized Hinotori satellite in situ measured electron density at 600 km altitude to derive a mean distribution of electron density at different local times. They compared their observations with the Sheffield University plasmasphere-ionosphere model (SUPIM), utilizing the EXB drift measured with the AE-E satellite and Arecibo incoherent scatter radar (ISR). Their results highlighted that a good model for EXB drift is the most important factor to explain the latitudinal distribution of the electron density. *Rama Rao et al*. [2006] also reported a significant correlation between the EIA crest amplitude and the strength of the EEJ. While the EEJ strength can be an important factor, the EXB drift measured using the ISR is likely to give a much more comprehensive explanation for EIA variability. *Stolle et al*. [2008] utilized Jicamarca Unattended Long-term Investigations of the Ionosphere and Atmosphere (JULIA) vertical plasma drift data to explain the daytime EIA variability. They utilized 5 years of Challenging Minisatellite Payload electron density data to infer the EIA strength. They found high correlation coefficient $cc > 0.8$ between JULIA EXB drift and EIA intensity. They also found the EIA response time to the changes in the EXB drift to be <2 h. On the other hand, the EIA response time to the changes in the EEJ strength was found to vary between 2 and 4 h. They also reported a complete absence of EIA on days with zero vertical EXB drift.

One of the most reliable techniques of measuring the vertical EXB drift is the incoherent scatter radar (ISR). It however, exists only at Jicamarca in the equatorial latitude. Doppler shifts of the daytime 150 km radar echoes have also been found to correlate well with the ISR. CINDI sensor on board the C/NOFS also measures the ion velocity. Recently, C/NOFS EXB drift has been found to agree well with the Jicamarca ISR vertical drift during the daytime [*Stoneback et al*., 2011]. C/NOFS EXB drift has also been found to correlate well with the EXB drift derived from 150 km echoes over Indian region [*Patra et al*., 2014]. C/NOFS EXB drift, however, has been found to correlate well with the ISR and 150 km echo drift only when the C/NOFS location was within $\pm 10°$ of the magnetic equator. Ionosondes (CADI, digisondes, and others), which are operational at more than 15 equatorial and low-latitude stations around the world, can also be operated in the fixed frequency mode to measure the Doppler shift of the reflected echo to derive EXB drift. Doppler measurement of the EXB drift in the HF frequency range (as in the ionosonde), during the daytime, however, is an underestimation of the actual EXB drift due to the photochemistry also controlling the height of the *F* layer [e.g., *Bertoni et al*., 2006]. The HF reflection occurs from an electron density value which corresponds to the plasma frequency, that is, the reflected frequency. During the daytime the height of the isoelectron density surface (the reflection height) is determined by the zonal electric field as well as the photochemistry (the ionization production and the recombination loss). Therefore, the Doppler velocity determined from the height changes is also subject to photochemistry influences during the daytime. As a result, the Doppler EXB drift measured in the HF band during the daytime is an underestimation of the actual vertical EXB drift. Thus, the ionosonde Doppler EXB drift must be corrected for the underestimation related to the photochemistry, before it can be utilized for ionospheric modeling and related applications.

In the present investigation, ionosonde-derived Doppler EXB drift has been compared with the C/NOFS vertical EXB drift, to figure out the correction that needs to be applied to the former in the daytime. The corrected ionosonde-derived vertical drift based on the artificial neural network has been utilized as an input to the SAMI2 model, to assess its utility in modeling the daytime EIA. SAMI2 model daytime ionospheric densities have been compared with the vertical total electron content (VTEC) map of international Global Navigation Satellite Systems (GNSS) service (IGS) over Indian longitude. An artificial neural network-based analysis for the correction of the daytime Doppler drift has also been developed.

2. Instrument Description, Data, Model, and Methodology

For the present investigation, ionosonde data from January–November 2012 period from Tirunelveli, a magnetic equatorial station in India, has been utilized. The ionosonde data corresponds to the fixed frequency Doppler sounding mode providing the vertical EXB drift. A Canadian advanced digital ionosonde (CADI), installed at Tirunelveli, was operated in 5 MHz fixed frequency Doppler sounding mode during January to November 2012. Data, however, were not continuous, and there were data gaps. Doppler sounding with CADI is a well-established technique to derive the vertical plasma drift of the *F* layer [*Cannon et al*., 1991; *Grant et al*., 1995; *Abdu et al*., 1998]. Doppler sounding technique used in the CADI to measure vertical EXB

drift is briefly described next. Receiving antenna array in the CADI system consists of four dipoles arranged along the sides of a square with length of 30 m. Each receiving dipole is attached to a separate receiver. Drift measurement is carried out at a rate of 0.016 Hz, i.e., once every 60 s. For that, a 64-point complex time series is generated every 60 s for each range bin of all the four antennas. Data integration is also carried out to reduce its storage size. This 64-point time series is Fourier transformed in real time for all the range bins of each antenna to generate power spectra. Least squares fitting is carried out to each power spectrum to make it smooth. The range bin with maximum received power is identified for the first antenna and is set for all the four antennas. Reliable Doppler shifts can be derived from the power spectrum only if the SNR is adequate. Thus, there can be a data gap in the Doppler measurement if the received power is not sufficient. Frequency bin in the power spectrum with the maximum power in all four antennas represents the Doppler shift of the received signal. Line of sight drift is calculated by multiplying the Doppler shift with half of the operating wavelength, $\lambda/2$. Thus, the method of calculating the Doppler drift in CADI system is quite similar to the one employed in a coherent scatter radar (CSR), except for the operating frequency. A CSR usually operates in the VHF frequency band, while CADI operates in HF frequencies in the range of 2 to 20 MHz; in present case 5 MHz carrier frequency has been utilized. For more literature on the ionosonde Doppler technique, one can refer to *Bibl and Reinisch* [1978], *Grant et al*. [1995], *Cannon et al*. [1991], and the references therein. However, during the daytime, vertical EXB drift inferred from the Doppler shift in the HF frequencies is an underestimation of the actual EXB drift due to the photochemistry also controlling the height of the *F* layer [*Woodman et al*., 2006; *Bertoni et al*., 2006].

Coupled Ion Neutral Dynamics Investigation (CINDI) on board C/NOFS also measures the EXB drift in the upward or the meridional direction [*Stoneback et al*., 2012]. CINDI payload includes the ion velocity meter which is utilized to measure the ion velocity. C/NOFS fly in a low inclination orbit of 13° and has an orbital period of 97.3 min. Its perigee is 405 km, and apogee is about 850 km. For further details about the CINDI payload one can refer to *Stoneback et al*. [2012]. C/NOFS EXB drift data of 2012 have also been utilized for the present study. C/NOFS data are available through an open repository (http://cdaweb.gsfc.nasa.gov/).

SAMI2 model has also been utilized to simulate the daytime EIA formation. SAMI2 is a versatile physics-based ionospheric model which simulates the chemical and dynamical evolution of the seven major ionic species along the entire magnetic flux tube [*Huba et al*., 2000]. SAMI2 model in its default form considers the vertical plasma drift to be defined by the EXB drift model [*Scherliess and Fejer*, 1999]. In the present study, the vertical EXB drift model in the SAMI2 has been replaced by the corrected ionosonde Doppler EXB drift, which is based on the neural network output. Thus, the applicability of the corrected ionosonde Doppler EXB drift for the daytime EIA modeling has been assessed. Thermospheric winds in the SAMI2 model are taken from HWM model, as in the default form of SAMI2 codes.

Latitudinal variation of the total electron content over the Indian longitude has also been derived from the global ionospheric map (GIM), distributed by NASA (ftp://cddis.gsfc.nasa.gov/gnss/products/ionex/) [e.g., *Lei et al*., 2008]. GIM is based on ~300 GPS sites of IGS and other institutions located around the world. Latitudinal variation of the TEC provides the structure of the equatorial ionization anomaly (EIA). EIA reproduced in the SAMI2 model has been compared with the observed EIA densities.

3. Results

3.1. EXB Drift Measurement Over Tirunelveli

The usual pattern of the zonal electric field (vertical EXB drift) over the equator is indicated by an eastward (upward) direction during the daytime and a westward (downward) direction during the night. Prior to the transition from the day to the night sector, the zonal eastward electric field shows an enhancement referred to as the prereversal enhancement (PRE) of zonal electric field. PRE of the zonal field transports the *F* layer to a very high altitude and plays a vital role in the generation of plasma irregularities also. The over plot of the diurnal vertical EXB drift recorded by the CADI installed at Tirunelveli (8.7°N, 77.7°E, 0.4° dip magnetic latitude) in the Doppler mode operating in 5 MHz HF frequency during 16 March 2012 to 30 April 2012 period is shown in Figure 1. Here each circle indicates the 15 min averaged EXB drift. Vertical EXB drift can be seen to be positive (upward) during the daytime and predominantly negative (downward) during the nighttime. Prior to the reversal of the direction of the vertical EXB drift in the postsunset period, there is a large enhancement in the EXB drift. Thus, the CADI in the Doppler sounding mode could record the features of the PRE of the zonal

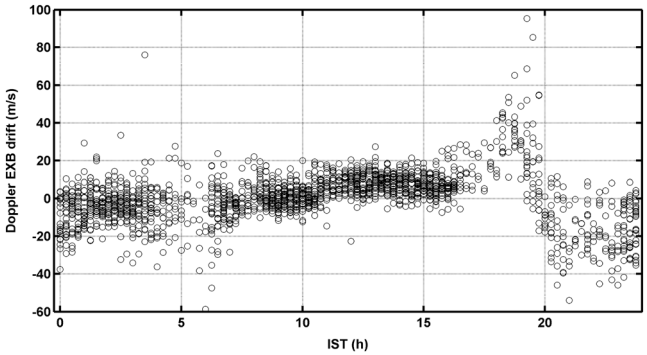

Figure 1. Vertical EXB drift measured using the Doppler sounding with Canadian Advanced Digital Ionosonde (CADI) from Tirunelveli, India, during 16 March 2012 to 30 April 2012 period. Here each circle indicates vertical EXB drift averaged over 15 min.

electric field. Another important aspect of the CADI observations is a very low EXB drift magnitude during the daytime in comparison with the postsunset time values owing to the PRE of the zonal field. The Doppler EXB drift during the daytime between 10 to 15 IST (here IST stands for the Indian standard time; IST = UT + 5:30 h; local time at Tirunelveli = IST − 18 min) can be seen to vary in the range of 0–20 m/s. These values are significantly less in comparison to the previously reported values of the daytime EXB drifts [*Scherliess and Fejer*, 1999]. It must be mentioned again that the Doppler EXB drifts measured in the HF frequencies during the daytime is an underestimation of the actual drifts due to the photochemistry that controls the height of the *F* layer [see *Bertoni et al*., 2006]. During the periods of the photo production, i.e., during the daytime, the reflection height of the *F* layer is not explicitly dependent on the EXB drift, which causes the underestimation in the vertical drift measurement in HF radio signals [*Bertoni et al*., 2006; *Woodman et al*., 2006]. Thus, some correction term must be identified that can be applied to the daytime Doppler EXB drift measured in the 5 MHz frequency.

3.1.1. Relation Between C/NOFS EXB Drift and the CADI EXB Drift During the Daytime

EXB drift measured using the CINDI payload on board C/NOFS has already been found to be in a good agreement with the Jicamarca ISR measurement and Gadanki/Kototabang 150 km echo measurement [*Stoneback et al*., 2011; *Patra et al*., 2014]. C/NOFS makes a maximum of 14 passes over a particular longitude sector in a day. Also, data gaps often exist due to the CINDI payload limitations [*Stoneback et al*., 2011, 2012]. Earlier investigations have indicated the CINDI EXB drift measurements to be a reliable mean of measuring the *F* layer vertical EXB drift but only during the periods C/NOFS flies within ±10° of the magnetic equator [*Stoneback et al*., 2011; *Patra et al*., 2014]. C/NOFS EXB drifts have not been found to agree well with the Jicamarca ISR drifts, and 150 km RADAR echo drifts when it flew over higher latitudes. It will be interesting to compare the C/NOFS EXB drift with the CADI EXB drift to quantify the underestimation of the daytime Doppler measurement in 5 MHz HF frequency. Figure 2 presents the correlation between the daytime C/NOFS EXB drift and the CADI EXB drift over Tirunelveli for the period 16 March 2012 to 30 April 2012. Only the EXB drift measurements corresponding to the occasion when the C/NOFS flew within ±10° of the magnetic equator has been considered for this comparison. Also, the 15 min averaged value of the CADI EXB drift has been used for the comparison. Figures 2a–2d present the comparison at 9–11 IST, 11–13 IST, 13–15 IST, and 15–17 IST, respectively. It shows a fair to good correlation between the two different techniques. Green line in the plots represents the linear best fit line and the equation mentioned in the plot represents the best fit line equation. One can note that the underestimation of the EXB drift using the CADI Doppler measurement varied with time. The underestimation was very significant during 9–11 IST, possibly due to the photo production dominating the height and the vertical structure of the ionosphere. The underestimation was not that significant during 15–17 IST when the photo production rate decreases with time and electric field starts playing a dominant role in determining the height of the *F* layer.

EEJ strength in terms of the difference in the horizontal magnetic field recorded at equatorial and off equatorial locations has been considered as a proxy for the zonal electric field, since a long time. *Anderson et al*. [2002], have indicated a linear relation between the Jicamarca EXB drift and the δH (difference in the horizontal component of the magnetic fields recorded at Jicamarca and Piura), which can also be utilized to derive vertical EXB drift considering the magnetic field recordings. Thus, the C/NOFS and ionosonde Doppler measurement of the EXB drifts have also been compared with the δH (difference in the horizontal component of the magnetic field recorded at Tirunelveli and Alibag), to further substantiate the observations. Figure 3 presents the relation between the C/NOFS EXB drift and the δH. It shows a linear relation as expected. Relation between the ionosonde Doppler EXB drift and the δH is shown in Figure 4. It also shows linearity between the

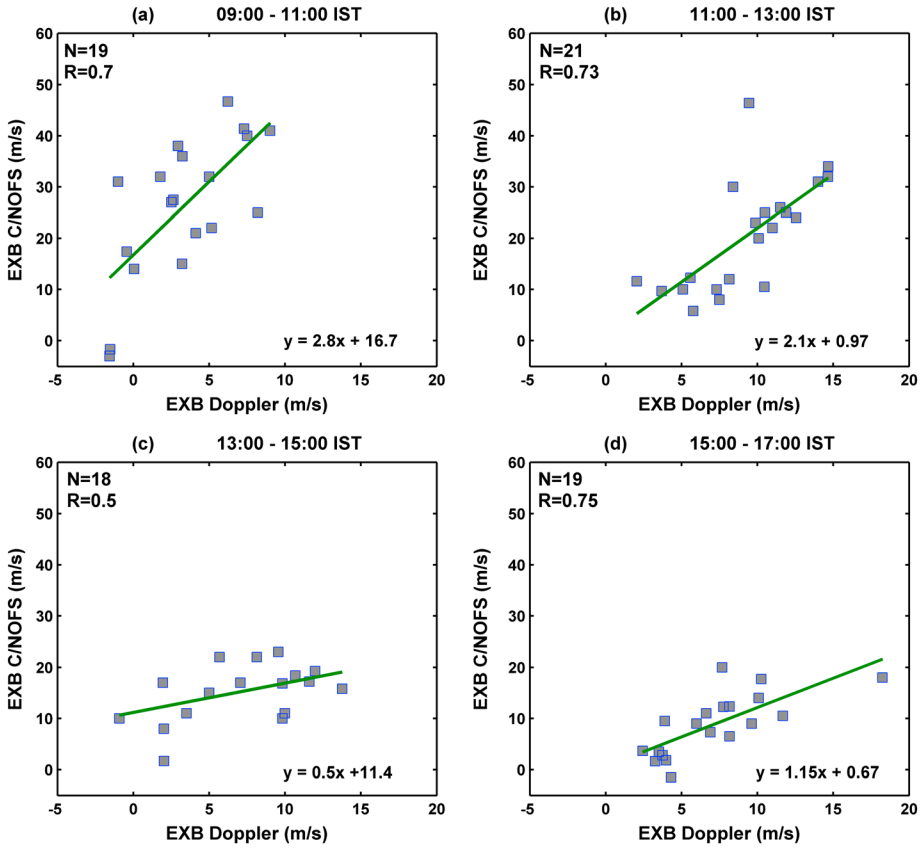

Figure 2. Comparison between the vertical EXB drift measured using the ionosonde Doppler and CINDI payload on board C/NOFS during 16 March to 30 April 2012 period, at (a) 09:00–11:00 IST, (b) 11:00–13:00 IST, (c) 13:00–15:00 IST, and (d) 15:00–17:00 IST. *N* and *R* indicate the number of samples and correlation coefficient, respectively. Green line shows the linear best fit relation, and the equation indicated in the plots presents the linear best fit line equation.

two. Thus, EXB drift in the equatorial region can also be derived using the ground-based magnetometer data [*Anderson et al.*, 2002, 2004].

Further in the investigation, time-dependent corrections have been applied to the CADI EXB drift, in accordance with the time-dependent relation presented in Figure 2. Corrections have been applied in accordance with the best fit line equations indicated in Figure 2. Also, an artificial neural network-based correction of the Doppler EXB drift during the daytime (09:00 to 17:00 IST) has been implemented. Neural network-based corrected EXB drift has also been used to simulate the EIA in the SAMI2 model. Examples of the correction applied to the CADI EXB drift are presented in Figure 5. In Figures 5a and 5b, EXB drift measured by the CADI on 16 March 2012 and 20 March 2012, respectively, is being presented. Here each green circle indicates the 15 min averaged EXB drift recorded by the CADI. Blue line indicates the interpolated, averaged and smoothed value of the CADI EXB drift. Time-dependent corrections based on the best fit line equations presented in the Figure 2 earlier have been applied on to the smoothed CADI EXB drift indicated by blue line in Figure 5. Corrected EXB drift is indicated with bold red line in Figure 5. Thick dashed black line in Figure 5 indicates the daytime (09:00 to 17:00 IST) EXB drift calculated based on a neural network approach, which will be discussed later in detail. The correction is quite significant during the early part of the daytime, and its significance was less after 15 IST. It is also interesting to see that the EXB drift based on neural network approach (as indicated by dashed black lines) indicates a higher value for the case where Doppler EXB drift was higher, i.e., 20 March 2012. Daytime EIA have also been simulated utilizing the neural network daytime EXB drift. Advantages of neural network approach will be discussed in detail later in the paper. SAMI2 model simulations are discussed next.

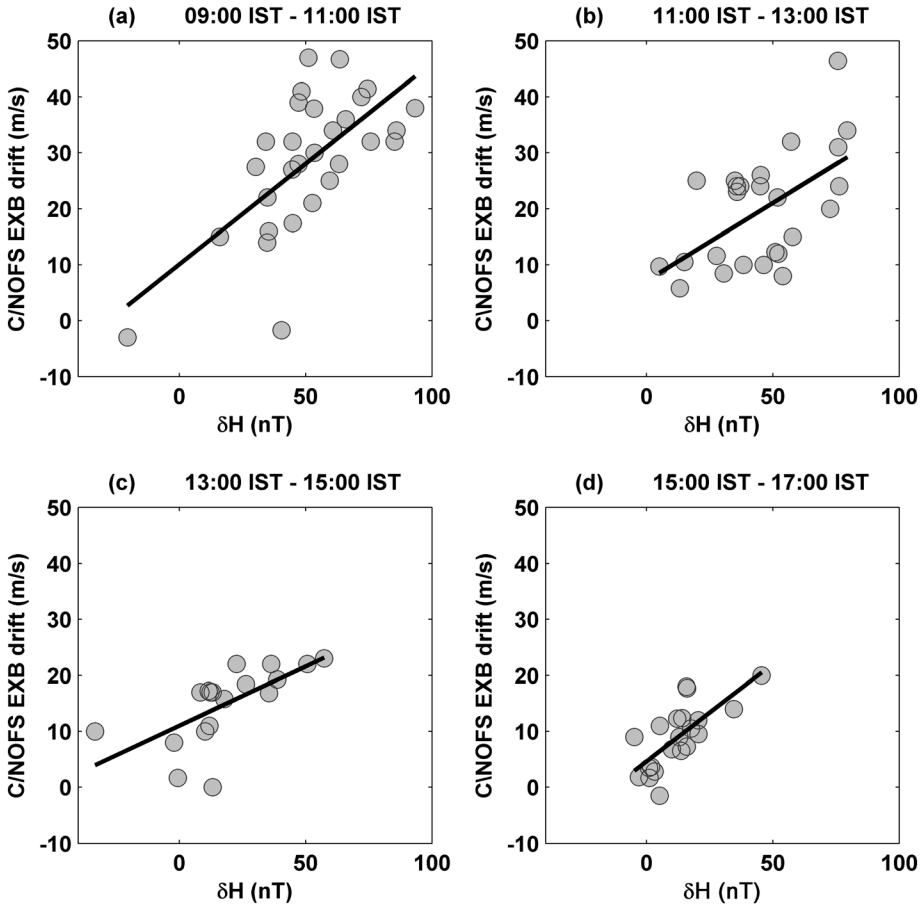

Figure 3. Relation between the vertical EXB drift measured using the CINDI payload on board C/NOFS and the difference between the horizontal component of the Earth's magnetic field recorded at Tirunelveli (equator) and Alibag (low latitude), δH, during 16 March to 30 April 2012 period at (a) 09:00–11:00 IST, (b) 11:00–13:00 IST, (c) 13:00–15:00 IST, and (d) 15:00–17:00 IST.

3.2. SAMI2 Modeling of the Daytime EIA

Primary driver of the daytime EIA is the zonal eastward electric field that pushes the ionospheric plasma upward. Plasma diffuses along the magnetic field lines to higher latitudes. This process is similar to a fountain. As the diffusion along the magnetic field line is a relatively slower process, the response of EIA to the eastward electric field appears after 1–2 h. In the SAMI2 model, the EXB drifts during 09:00 to 17:00 IST have been taken from the neural network (as shown in dashed line in Figure 5), while the Doppler EXB drift have been utilized during the remaining hours of the day. Meridional neutral wind in the SAMI2 model, however, has been taken from the HWM model (as in the default version of SAMI2). Figure 6 presents the SAMI2 model latitudinal-altitudinal distribution of the ionospheric plasma on 16 and 20 March 2012. Here Figures 6a–6d indicate the latitudinal-altitudinal distribution of the ionospheric plasma on 16 March 2012 at 12, 14, 16, and 18 IST, respectively. Figures 6e–6h indicate the same, but for 20 March 2012. While the anomaly formation took place on both the days, its strength was significantly larger on 20 March 2012. While the EIA can be seen in both the cases, its expanse is different in the two cases. On 20 March the crest-trough latitudinal separation is quite large in comparison to that on 16 March. Thus, the differences in the neural network EXB drift for the two cases have reproduced significant difference in the ionospheric redistribution in SAMI2 model. Another important aspect seen here is the maintenance of EIA in the sunset hours. Clearly defined crest/trough can be seen at 18 IST on both days. This is also in part due to the maintenance of the fountain effect driven by the PRE of zonal field. Several earlier studies have reported the enhancement of the EIA in the postsunset hours due to the PRE of zonal field [e.g., *Whalen*, 2004; *McDonald et al*., 2011].

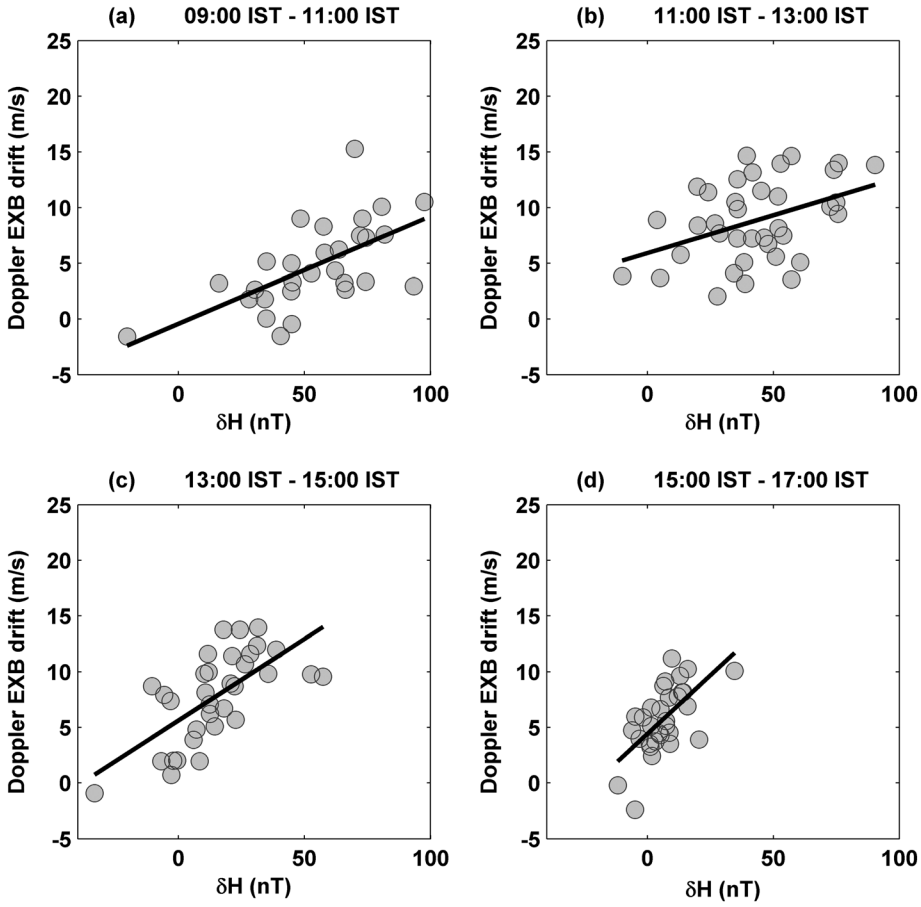

Figure 4. Relation between the ionosonde Doppler EXB drift and the difference between the horizontal component of the Earth's magnetic field recorded at Tirunelveli (equator) and Alibag (low latitude), δH, during 16 March to 30 April 2012 period at (a) 09:00–11:00 IST, (b) 11:00–13:00 IST, (c) 13:00–15:00 IST, and (d) 15:00–17:00 IST.

The total electron content has also been calculated based on the SAMI2 model. Figures 7a and 7b show the vertical TEC during the daytime on 16 and 20 March 2012, respectively. Here the vertical TEC has been calculated by integrating the plasma density vertically from 100 km to 1200 km altitude. There can be seen a remarkable difference in the TEC modeled on the two days. EIA strength based on the modeled TEC was quite remarkable on 20 March 2012. While the peak TEC was in the range of 80–100 TECU on 20 March 2012, it was less than 70 TECU in the anomaly crest region on 16 March 2012, clearly showing the important role EXB drift can play in determining the low-latitude TEC and its variability.

3.3. Case Studies

A detailed case study is presented for the days when the daytime Doppler EXB drift was the lowest during 16 March 2012 to 30 April 2012 period. These cases have also been compared with the days when the daytime EXB drift were maximum during the same period. Thus, the extreme cases of the least and the highest values of the daytime EXB drift are being compared to understand, in detail, their impact on the ionospheric densities. Figure 8 shows the six cases of lowest and six cases of the highest daytime EXB drift recorded during 16 March 2012 to 30 April 2012 period. These also include the two cases discussed earlier in Figure 5. Figures 8a–8d indicate the 15 min averaged Doppler EXB drifts, smoothed Doppler EXB drifts, corrected Doppler EXB drifts (based on linear regression presented in Figure 2), and daytime (09:00 to 17:00 IST) EXB drift based on neural network approach, respectively, for the cases with least daytime Doppler EXB drift values. Figures 8d–8f indicate the same, but for the cases with highest daytime Doppler EXB drift during the same period. Dates of the cases are indicated with a unique color in each category. Corrected EXB drift based on linear regression analysis indicated in the Figures 8c and 8g shows a remarkable difference in

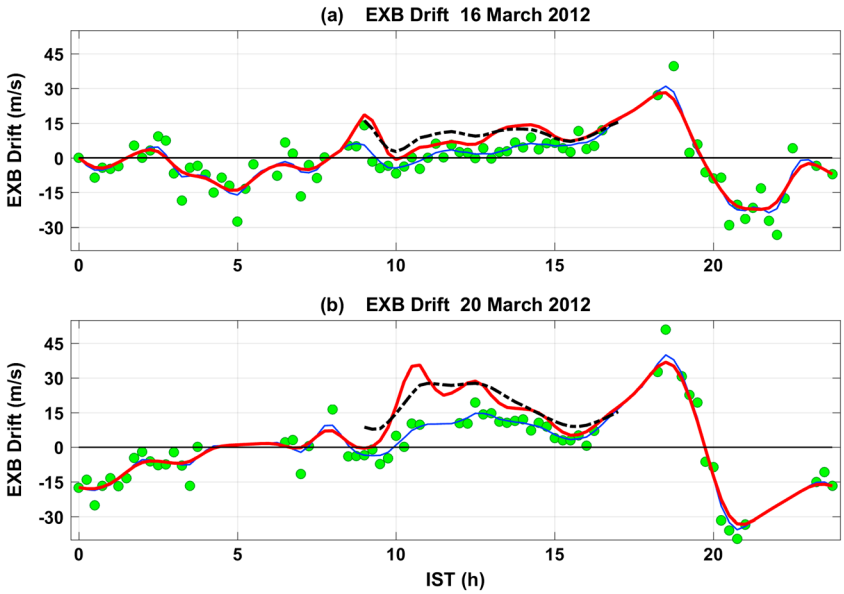

Figure 5. Doppler EXB drift recorded over Tirunelveli (a) on 16 March 2012 and (b) on 20 March 2012. Here each green circle indicates 15 min averaged Doppler EXB drift. Blue line indicates the interpolated and smoothed Doppler EXB drift. Thick red line indicates the corrected Doppler EXB drift (based on linear regression). Black dashed line indicates the EXB drift derived from neural network during the daytime (09:00 to 17:00 IST). Details are given in the text.

the two categories. Daytime EXB drift calculated based on a neural network-based analysis, as indicated in Figures 8d and 8h, also shows a remarkable difference in the two categories. The peak daytime EXB drift based on neural network in the first category was in the range of 10–20 m/s, while it was more than 30 m/s in the second category. Neural network-based approach, which will be discussed in detail later in the paper, based on highly nonlinear mapping, considers several factors like season (day of the year), solar ($F_{10.7}$), and geomagnetic conditions to correct the ionosonde Doppler drift against underestimation. Daytime VTEC modeling based on the neural network EXB drift is presented next.

3.3.1. Modeling the TEC for Low and High EXB Drift Cases

Daytime neural network EXB drifts indicated in the Figures 8d and 8h for the two categories have been used as input vertical EXB drift to the SAMI2 model during 09:00 to 17:00 IST to understand their relative impact in the formation of the EIA during the daytime. During remaining hours of the day, EXB drift in the SAMI2 model have been considered based on Doppler measurement (as SAMI2 model run requires diurnal EXB drift to be defined). Vertical TEC has been computed from the SAMI2 model output for the two categories. Figure 9 shows the vertical TEC based on SAMI2 model for the two categories. Figures 9a–9f indicate the VTEC for the six cases with least daytime EXB drift, while the right panels indicate the VTEC for the six cases with highest EXB drift. Two of the important features of the VTEC in the two categories are as follows: (1) the EIA strength is much higher in the high EXB drift cases than in the low EXB drift cases, and (2) the difference in the peak TEC in the two categories is of the order of 20–30 TEC units. The EIA strength is related to the difference in the TEC between the crest and the trough. The peak TEC depends upon the transport and also the loss process of the ionization. Both the transport (fountain effect) and the recombination rate (height dependent) will be favorable for high TEC values when EXB drift is higher. Thus, under large daytime EXB drift conditions, both the TEC and its latitudinal distribution are quite significant.

3.3.2. Total Electron Content Over Indian Longitude Based On GIM

Global ionospheric map or GIM provides a convenient tool to study the latitudinal-longitudinal distribution of the ionospheric TEC. GIMs are based on TEC measurements at more than 300 GNSS stations of the IGS and other institutions located around the world. GIM provides the TEC value with a coarse latitudinal and longitudinal resolution of 2.5°, interpolating the TEC values between the recording stations using suitable method. GIMs are updated every 2 h. GIMs are intended to provide a global coverage and are somewhat less efficient than the dedicated regional networks like GAGAN (GPS Aided Geo Augmented Navigation) and Wide Area Augmentation System. Nonetheless, GIMs do provide an efficient tool to study the latitudinal distribution

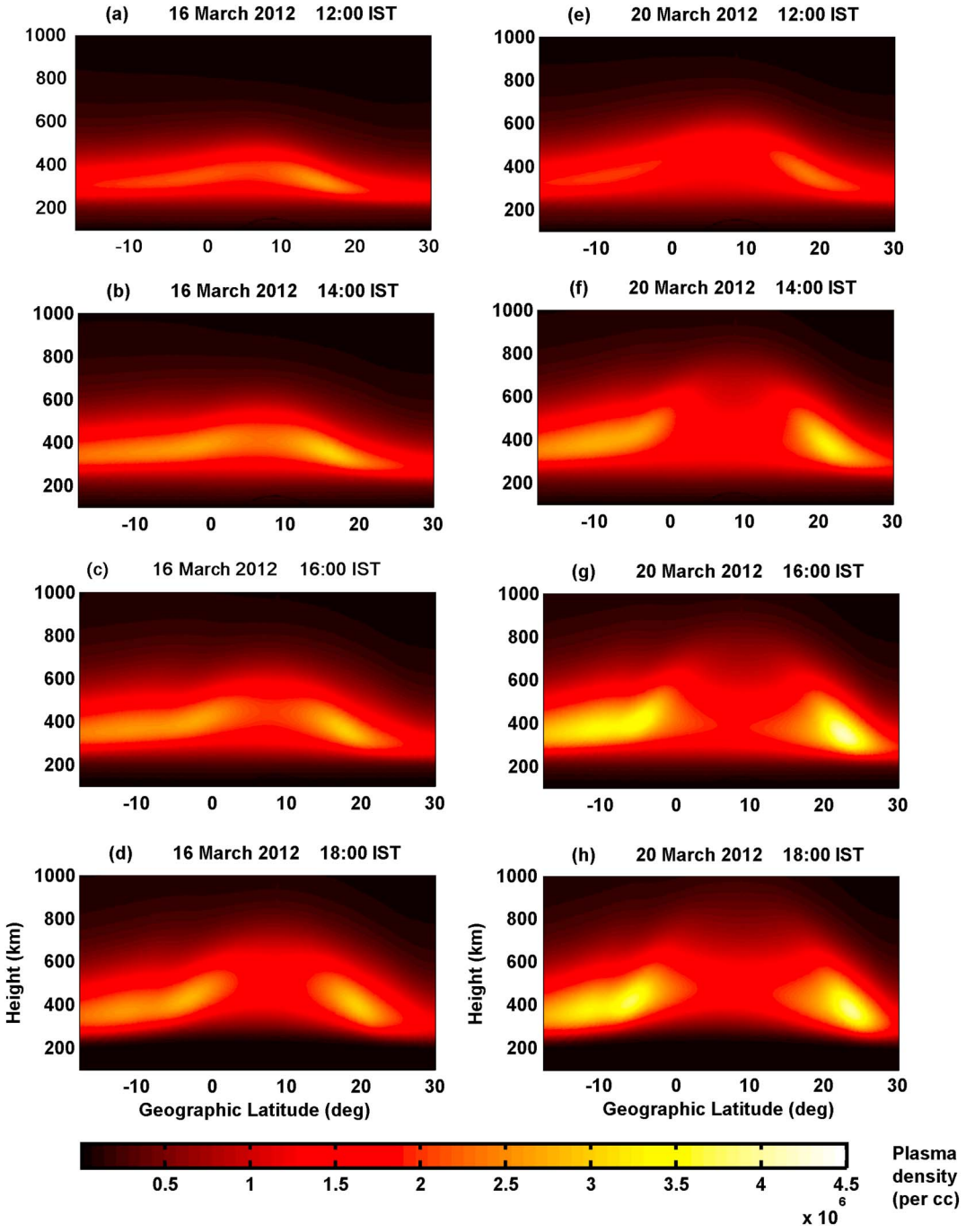

Figure 6. (a–d) Latitudinal-altitudinal distribution of the ionospheric plasma over Indian longitude in the SAMI2 model on 16 March 2012 at 12 IST, 14 IST, 16 IST, and 18 IST, respectively. (e–h) Same as Figures 6a–6d, but on 20 March 2012.

of TEC [*Ho et al.*, 1997; *Mannucci et al.*, 1998; *Buonsanto*, 1999; *Iijima et al.*, 1999; *Kil et al.*, 2003; *Zhao et al.*, 2007; *Lei et al.*, 2008; *Wan et al.*, 2008; *Uma et al.*, 2012]. Also, the GIM data are openly accessible to researchers unlike the GAGAN data. The IGS stations located within the expanse of the Indian longitudes that go into the construction of GIMs are as follows: Lhasa (29.6°N, 91.1°E), Lucknow (26.9°N, 80.9°E), Hyderabad (17.4° N, 78.5°E), Bangalore (13.0°N, 77.5°E), Maldives (4.1°N, 73.5°E), and Diego Garcia (−7.2°N, 72.3°E). Out of these, Lucknow, Hyderabad, and Bangalore are located in India. While stations Lhasa and Lucknow are located beyond the northern crest of the EIA, Hyderabad is located at the northern crest of the EIA. Stations Bangalore and Maldives are located 4° northward and southward, respectively, of the trough of the EIA.

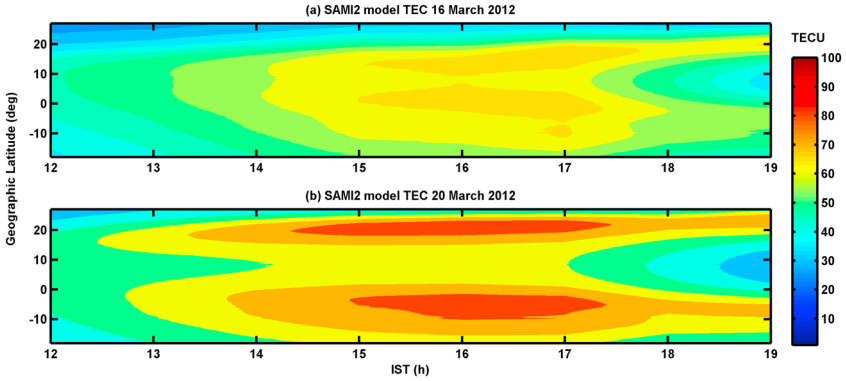

Figure 7. Total electron content calculated from SAMI2 model on (a) 16 March 2012 and (b) 20 March 2012.

Diego Garcia is located 2°–3° southward of the southern crest of the EIA. Thus, in the vicinity of the Indian longitudes, IGS stations are located close to the EIA crest and trough regions.

Figure 10 shows the TEC variation over the Indian longitude based on the GIMs, corresponding to the low and high EXB drift cases discussed in Figure 8. Figures 10a–10f present the TEC variation over the Indian low

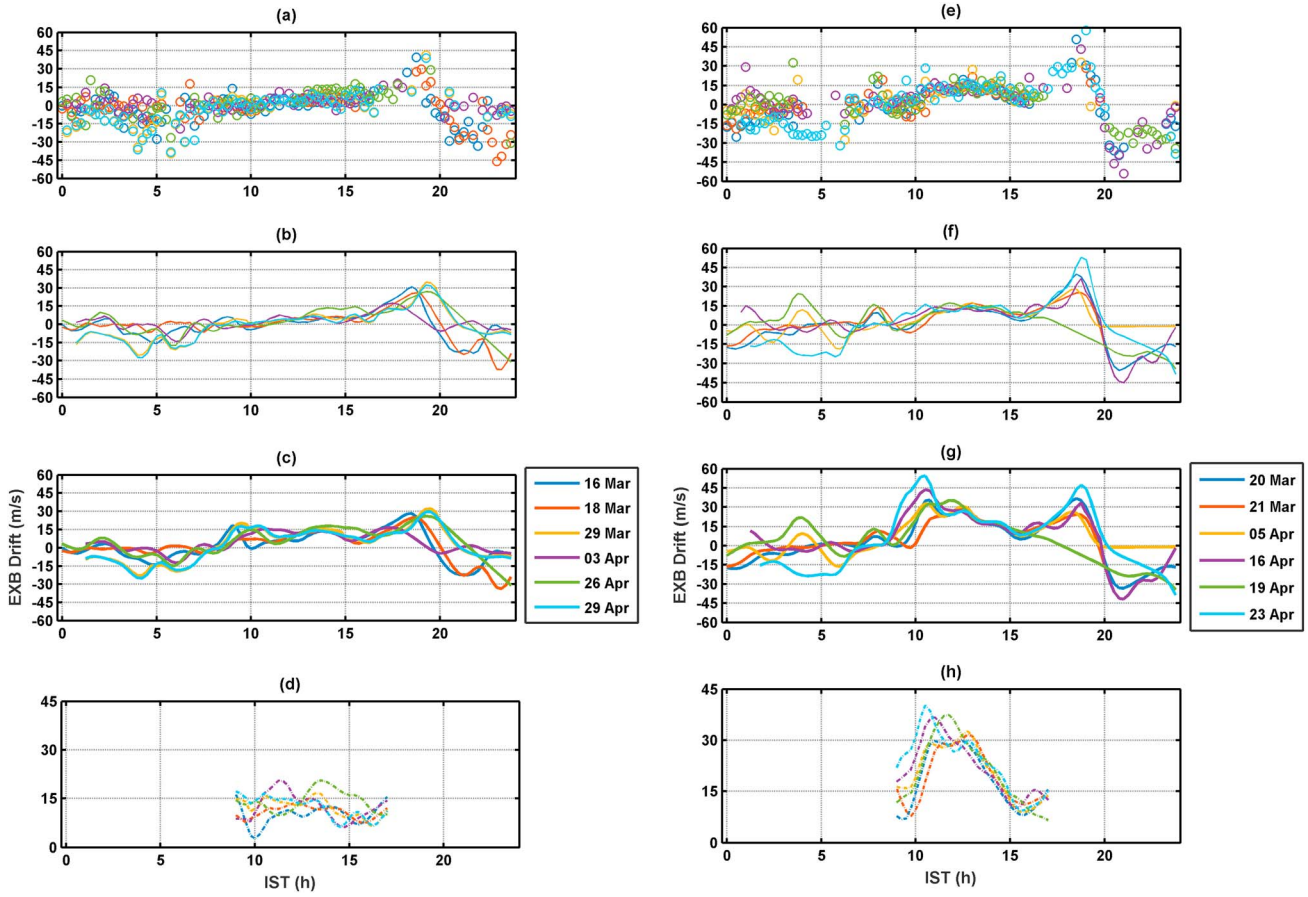

Figure 8. Detailed case study during 16 March to 30 April 2012 period. (a–d) Ionosonde Doppler EXB drift corresponding to six low daytime drift cases. Figures 8a–8d show 15 min averaged Doppler EXB drift, smoothed Doppler EXB drift, corrected Doppler EXB drift (based on linear regression), and neural network daytime EXB drift, respectively, for the six low daytime EXB drift cases. (e–h) Ionosonde Doppler EXB drift corresponding to six high daytime EXB drift cases. Figures 8e–8h show 15 min averaged Doppler EXB drift, smoothed Doppler EXB drift, corrected Doppler EXB drift (based on linear regression), and neural network daytime drift, respectively, high daytime EXB drift cases.

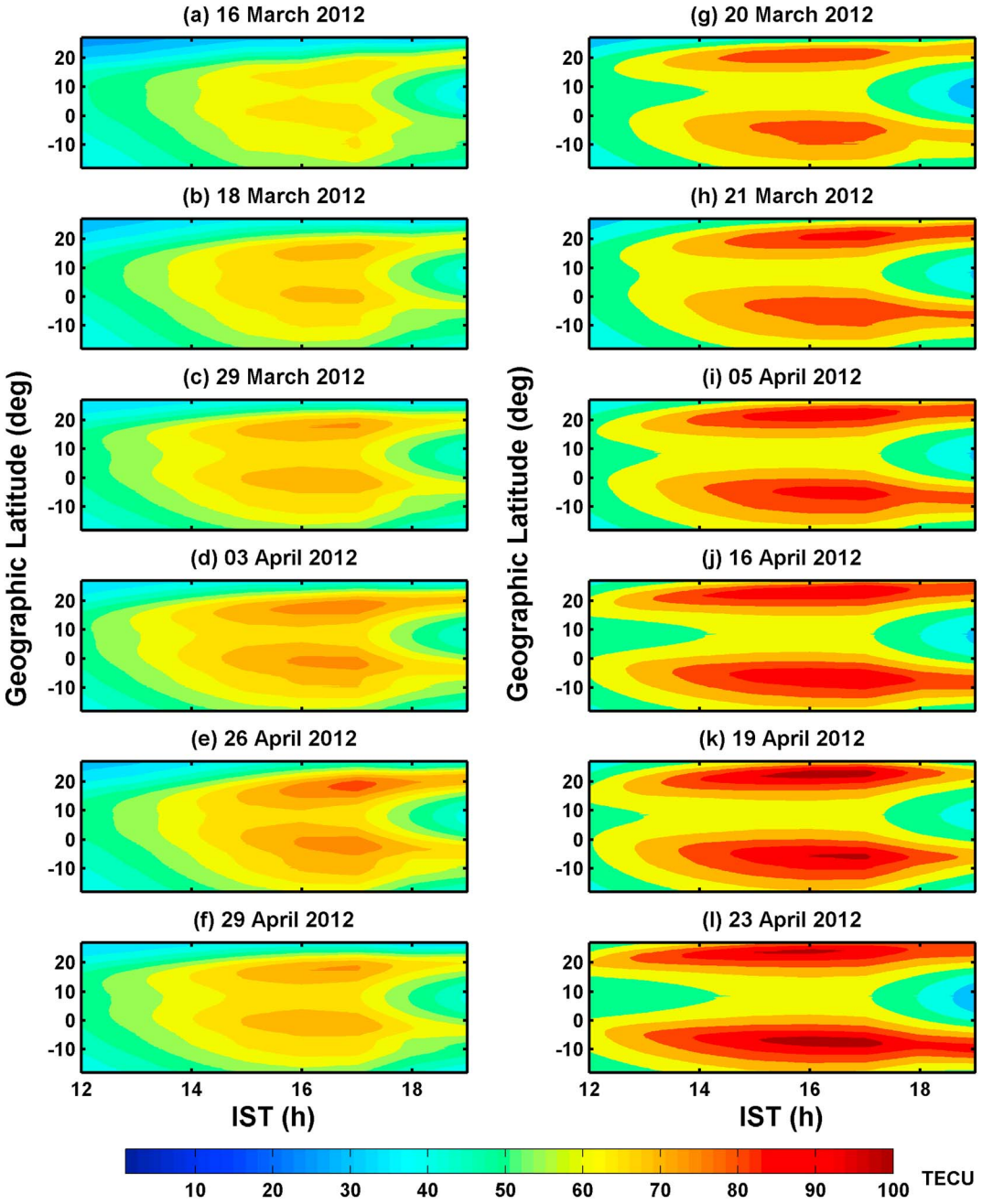

Figure 9. SAMI2 model TEC corresponding to the six low and six high daytime EXB drift cases discussed in Figure 8. (a–f) The SAMI2 model TEC corresponding to the six low daytime EXB drift cases. (g–l) The same, but corresponding to the six high daytime EXB drift cases.

latitude for low daytime EXB drift cases, while Figures 10g–10l indicate the same, but for the high daytime EXB drift cases. Well-defined EIA crest and trough regions can be seen in the right panels. In the left panels, EIA crest and trough are either completely absent or not well defined or highly discontinuous. Also, the plasma density in the anomaly trough region was much lower in the rightside cases than in the leftside cases. It seems evident that in the low EXB cases, the TEC recorded at stations located a few degrees away from the EIA trough, i.e., Bangalore and Maldives, was similar to the TEC recorded over the stations located in the close vicinity of the EIA crest. Thus, in the TEC maps the EIA was suppressed, possibly linked to the suppression of the plasma fountain owing to low daytime EXB drift. In contrast, in high EXB cases, the EIA crest/trough were clearly defined, indicating a greater distribution of the ionospheric plasma due to the plasma fountain.

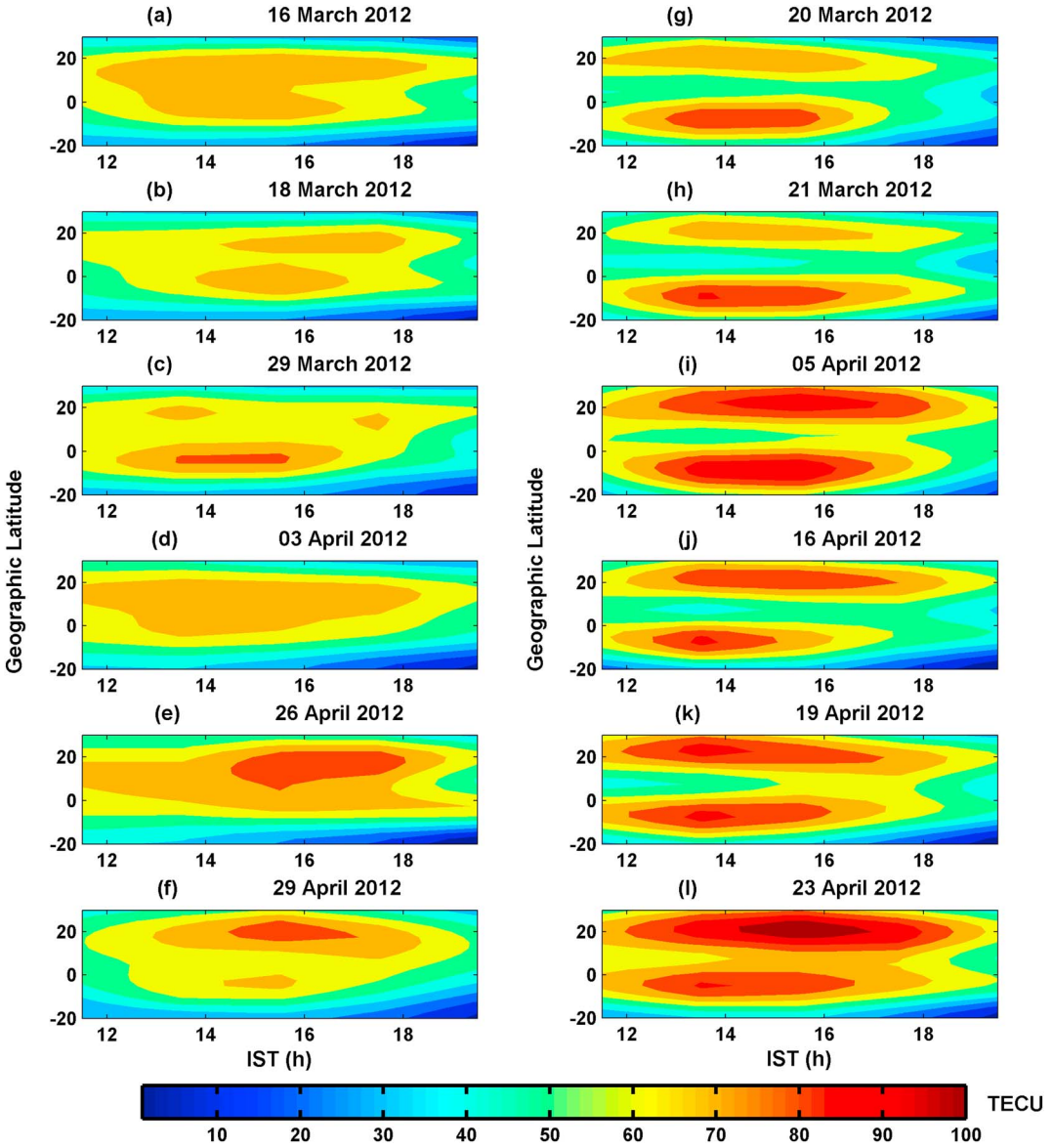

Figure 10. GIM TEC variation over Indian longitude corresponding to the six low and six high daytime EXB drift cases discussed in Figure 8. (a–f) The TEC corresponding to the six low daytime EXB drift cases. (g–l) The same, but corresponding to the six high daytime EXB drift cases.

3.4. Intraannual Variations in the Relation Between C/NOFS and CADI Doppler EXB Drifts

So far in the paper, EXB drift during 16 March 2012 to 30 April 2012 period has been discussed. However, the role of the photochemistry in the underestimation of the EXB drift measurement using CADI Doppler can vary with seasons. Vertical EXB drift not only displays a diurnal variation but also has intraannual variability [*Scherliess and Fejer*, 1999]. The underestimation in the measurement of vertical EXB drift measured in the HF frequency during the daytime is also likely to vary with the seasons due to the variation in the photo chemistry. The solar azimuth angle varies with months of the year and can play an important role in the ionospheric photochemistry. Also, the solar flux in the EUV and X-Ray range may vary. Thus, the relation between the satellite in situ EXB drift and ionosonde Doppler EXB drift might change with the seasons of the year. Figure 11 presents the relation between the daytime C/NOFS and Doppler EXB drifts at five different bimonthly/trimonthly epochs in 2012. Figures 11a–11d indicate the relation at 09:00 to 11:00 IST, 11:00 to 13:00 IST, 13:00 to 15:00 IST, and 15:00 to 17:00 IST, respectively. In Figure 11 R indicates the correlation coefficient, and thick lines represent the linear best fit lines. It must be mentioned that the June and December months cannot be compared in Figure 11 because of the complete gap in the

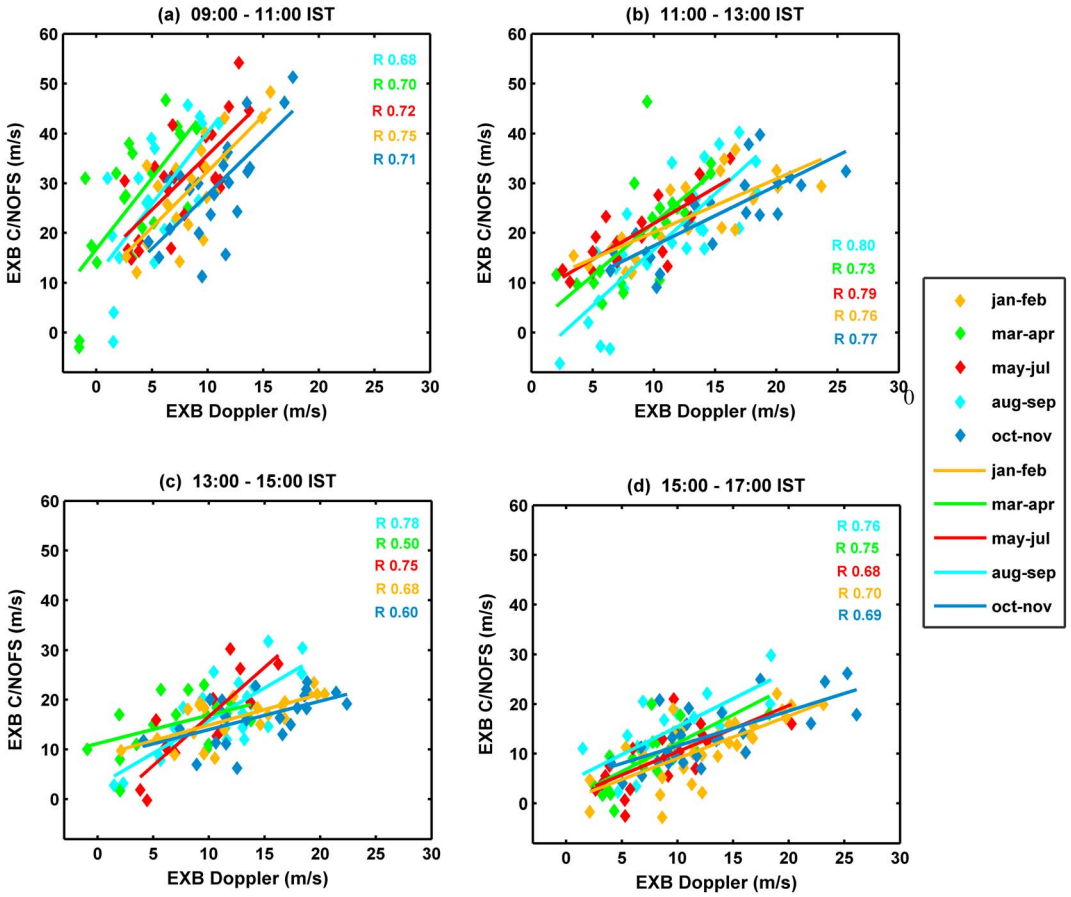

Figure 11. Relation between the CADI Doppler EXB drift and C/NOFS EXB drift in different bimonthly/trimonthly epochs.

ionosonde Doppler data in that period. The RMS errors for different bimonthly/trimonthly and local time epochs are indicated in Table 1. Two of the important points that can be noted from Figure 11 are as follows: (a) the underestimation is most severe during 09:00 to 11:00 IST which becomes lesser as the day progresses in all bimonthly/trimonthly epochs, and (b) the slope of the best fit line and the underestimation of the Doppler EXB drift in a particular time interval were different in different bimonthly/trimonthly epochs. This shows that the linear relation for the correction of the Doppler EXB drift varies with different months of the year. Thus, the underestimation will vary with local time, month of the year, solar activity, and possibly the longitude. Also, the EXB drift vary with season, and the influence of these factors on the EXB drift would be different than those on the photochemistry. To solve such a complex relation, the artificial neural network-based approach is likely to provide the most efficient results. *Anderson et al.* [2004] have found that the neural network-based solution provides a better estimation of the EXB drift from ground-based magnetometer observations, than a linear regression-based technique. Thus, a neural network-based analysis have been performed to correct the Doppler EXB drift during the daytime (09:00 to 17:00 IST) against the underestimation.

Table 1. RMS Error in the Regression Analysis for Different Bimonthly/Trimonthly Epochs

	RMS Error (m/s) at Different Months and Local Time Intervals				
Time Intervals	Jan–Feb	Mar–Apr	May–Jul	Aug–Sep	Oct–Nov
09:00–11:00 IST	7.28	7.66	7.41	7.18	6.94
11:00–13:00 IST	6.59	6.62	5.91	5.83	6.32
13:00–15:00 IST	5.31	5.34	5.25	5.17	5.21
15:00–17:00 IST	4.3	5.33	4.83	4.91	5.28
Overall RMS error			5.93		

3.5. Neural Network Approach to Data Analysis

Neural network-based correction of the daytime Doppler EXB drift (which has also been used to simulate the EIA in SAMI2 in Figure 9) is being presented now. Feed forward neural network is a class of artificial

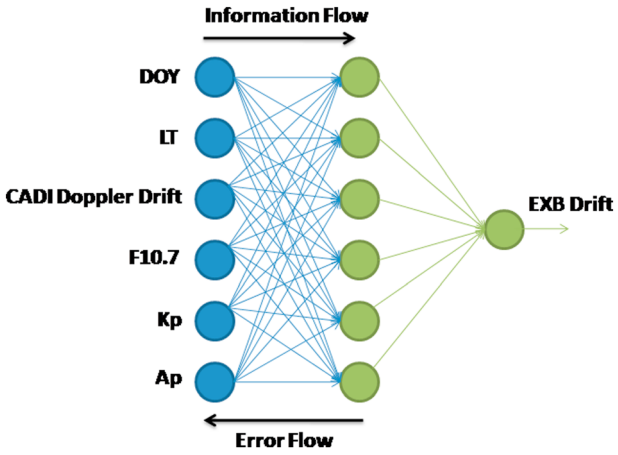

Figure 12. Feed forward neural network schematic.

neural network where links between different layers are noncyclic. These are the simplest form of artificial neural networks utilized for data fitting and function-approximation applications [*Sivanandam and Deepa*, 2006; *Gurney*, 1997]. It usually consists of an input layer and an output layer with one or more hidden layer sandwiched between the two. Each layer is connected to the other with at least one neuron. Each neuron has a nonlinear activation function except the one from input layer. Also, the different layers of this network are connected through a set of weights. Because of a highly distributed structure, feed forward neural network is able to reproduce a highly nonlinear mapping between the input and the target values. If a neural network consists of an input layer and an output layer connected with neurons having linear activation function, it will approximate a regression analysis.

Prior to its application, a feed forward neural network is required to be trained using the sample data. Training data set consists of a set of input values and also a set of desired output values. Entire input data sets are one by one fed in to the neural network, and the output set is obtained. This output set of values is then compared with the desired output values, and the errors are estimated. Once all the samples of the input data sets are shown to the network, a back propagation algorithm fixes the network weights so as to reduce the mean square errors between the output produced by the network and the desired output. Such training epochs are repeated till the mean square error between the network output and the desired output gets minimized. Several back propagation algorithms exists; however, Levenberg-Marquardt algorithm is known to reduce errors in lesser number of training epochs. For the neural network analysis presented in this paper Levenberg-Marquardt algorithm has been utilized for training as it has been found to produce the best results in terms of the mean square error. Network corresponding to the training epoch which produces the least mean square error is utilized as the trained network. This trained network can then be utilized for user applications.

In this paper, a neural network with one hidden layer with six neurons has been utilized. This scheme has been adopted as it was found to generate the best performance in terms of RMS error. Six input variables have been utilized as input to find out the nonlinear relation between the input and the output. The input variables are as follows: Day of the year (DOY), local time (LT), CADI Doppler drift, $F_{10.7}$, *Kp* and *Ap*. The target variable in the neural network was the EXB drift measured by the C/NOFS. A schematic of the neural network utilized in this study is shown in Figure 12. Total number of training samples was 480 (with 6×480 inputs and 1×480 target values), and entire set of samples has been used to train the network. The training phase of the neural network is indicated in Figure 13. Here zeroth training epoch indicates a perfectly untrained network with very high RMS error. This RMS error starts becoming lesser and lesser as training progresses. The training stops after RMS errors do not indicate a reduction, and the network at that point is considered trained.

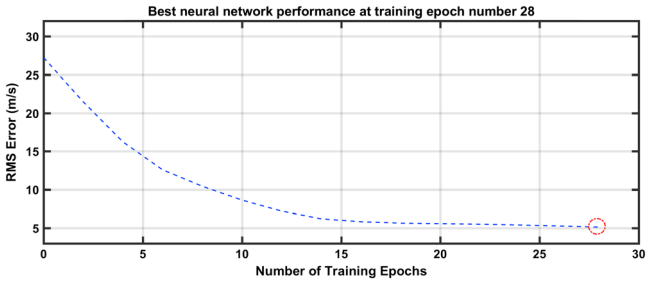

Figure 13. Training performance of the neural network.

The best neural network performance in Figure 13 happened in the training epoch number 28. The RMS error of the trained neural network is 5.1 m/s. The overall RMS error in case of the linear regression analysis, as shown earlier in Table 1, was 5.93 m/s. The neural network analysis has produced a lesser RMS error and thus is more efficient than linear regression analysis in totality.

4. Discussion and Summary

Vertical EXB drift measurement in the daytime using the fixed frequency ionosonde Doppler technique suffers from an underestimation of the actual EXB drift. Ionosonde Doppler measurement is considered reliable in the evening and postsunset hours; however, observations reveal that it severely underestimates the EXB drift in the periods of solar photoionization, i.e., daytime [*Woodman et al*., 2006; *Bertoni et al*., 2006]. Ionosonde measures the vertical drift based on the Doppler detection of the reflected echoes (unlike the scattered echoes, as in the case of coherent scatter radar or incoherent scatter radar). The HF reflection occurs from an altitude where electron density value corresponds to the plasma frequency, i.e., the reflected frequency. The height of the isoelectron density surface (the reflection height) is determined by the electric field as well as the photochemistry (the ionization production and the recombination loss). Thus, the Doppler velocity determined from the height changes is also subject to photochemistry changes during the daytime. *Yue et al*. [2008] found the ionosonde-derived vertical EXB drift to agree well with the model vertical EXB drift during the 0600–0730 and 1700–2100 local time. They also reported that the daytime vertical EXB drift inferred using the ionosonde during the magnetically disturbed period shows the features of the prompt penetration electric field and disturbance dynamo electric field. However, the magnitude of the ionosonde-derived vertical EXB drift remains less than that of the disturbed period model EXB drift. Recently, *Adeniyi et al*. [2014] have compared the ionosonde seasonal average vertical EXB drift over Ilorin, Nigeria, with the seasonal average Jicamarca ISR/150 km echo drift and with the model EXB drift. They have also reported the daytime ionosonde-derived vertical EXB drift to be significantly less than the Jicamarca EXB drift.

In the present investigation, an effort has been made to correct the ionosonde Doppler EXB drift against underestimation. A fair to good correlation was seen between the C/NOFS vertical EXB drift and the Doppler EXB drift during the daytime. Detailed relations between the C/NOFS and Doppler EXB drift during different bimonthly/trimonthly epochs have also been presented. Linear best fit line was found to vary significantly in different epochs. This indicated that the underestimation in the Doppler EXB drift varied significantly with seasons. Thus, seasonal, solar, and geomagnetic variables need to be considered to correct the Doppler EXB drift in a more efficient manner. Although the underestimation in the Doppler EXB drift varied most significantly with the local time, nonetheless, the contribution from other factors cannot be ignored. As reported in previous investigations [e.g., *Anderson et al*., 2004], neural network-based analysis provides the best means of estimating the EXB drift based on multiparametric input. Thus, neural network-based approach has been adopted to derive the EXB drift during the daytime using the six input variables. Neural network-based analysis resulted in the reduction of the RMS error. The overall RMS error in the regression analysis was 5.93 m/s, which was reduced to 5.1 m/s in the neural network-based approach. This further indicates that the neural network provides the best means of estimating the daytime EXB drift. *Anderson et al*. [2004] reported an RMS error of 3.79 m/s and slightly less than 3 m/s using regression and neural network method, respectively. Thus, the RMS errors reported in this work are somewhat higher than that of *Anderson et al*. [2004]. Possibly, these higher values are due to the presence of random noise in the data. *Anderson et al*. [2004] have utilized δH and 150 km echo drift from Jicamarca to figure out the relation between δH and the EXB drift. However, in this investigation CADI Doppler data have been utilized, which is likely to have more noise due to low operating power (in comparison to Jicamarca/JULIA radar); same may be the case with C/NOFS measurement, too. Nonetheless, the analysis presented in this paper clearly indicates that the ionosonde Doppler EXB drift in the daytime can be utilized to derive actual EXB drift in addition to the known technique of using the ground-based magnetometers [*Anderson et al*., 2002, 2004].

Thus, proper analysis of the network of equatorial ionosondes can be used to derive the global equatorial vertical EXB drifts, with excellent spatial and temporal resolution (more than 15 CADI/digisondes are operational in the equatorial regions around the world). Global EXB drift can then be utilized in three-dimensional ionospheric models like SAMI3. Also, the EXB drift is one of the most important components in the Global Assimilation of Ionospheric Measurements (GAIM) model [*Schunk et al*., 2004] aimed at enhancing the accuracy of the satellite-based global navigation systems. Any assimilative ionospheric modeling of navigational errors in regional satellite navigation systems in low latitudes will also require the continuous vertical EXB drift input as its integral component. Thus, ionosonde systems can also play an important role in deriving the daytime vertical EXB drift in the absence of ISR/CSR.

The investigations presented in this paper can be summarized as follows. Simultaneous C/NOFS and ionosonde observations of the vertical EXB drift over Tirunelveli have been utilized to correct the ionosonde Doppler EXB drift against underestimation during the daytime, based on feed-forward neural network analysis. Ionospheric modeling using SAMI2 model with neural network EXB drift as input has also been presented. The daytime EXB drift underestimation in the ionosonde Doppler measurement was found to vary with bimonthly/trimonthly epochs in 2012. Artificial neural network-based estimation of EXB drift resulted in a reduction in the overall RMS error in comparison to linear regression analysis. The results presented in this paper confirm that the daytime vertical EXB drift measured using ionosondes can be considered reliable, provided suitable corrections are applied to it.

Acknowledgments

One of the authors (L.M.J.) is thankful to Indian Institute of Geomagnetism Mumbai, India, for providing the "Nanabhoy Moos" Research Fellowship (Post Doctoral Fellowship). CINDI data used in this paper can be obtained from Coordinated Data Analysis Web (http://cdaweb.gsfc.nasa.gov/). CADI ionosonde data used in this manuscript can be obtained by contacting S. Sripathi or L. M. Joshi (lmjoshinarl@gmail.com). Authors are thankful to the technical staff of EGRL, Tirunelveli, for operating and maintaining the CADI. Global ionospheric TEC maps are available through a NASA repository (ftp://cddis.gsfc.nasa.gov/gnss/products/ionex/). This work uses the SAMI2 ionosphere model written and developed by the Naval Research Laboratory. SAMI2 codes have been modified to incorporate the measured EXB drift. SAMI2 codes are available at NRL website (http://www.nrl.navy.mil/ppd/branches/6790/sami2). EEJ strength data utilized in this paper are obtained from ODA group (Indian Institute of Geomagnetism). Authors would like to thank D. S. Ramesh, Director of IIG, for his kind support and encouragement.

References

Abdu, M. A., G. O. Walker, B. M. Reddy, J. H. A. Sobral, B. G. Fejer, T. Kikuchi, N. B. Trivedi, and E. P. Szuszczewicz (1990), Electric field versus neutral wind control of the equatorial anomaly under quiet and disturbed condition: A global perspective from SUNDIAL 86, *Ann. Geophys.*, *8*, 419–430.

Abdu, M. A., P. T. Jayachandran, J. MacDougall, J. F. Cecile, and J. H. A. Sobral (1998), Equatorial *F* region zonal plasma irregularity drifts under magnetic disturbances, *Geophys. Res. Lett.*, *25*(22), 4137–4140, doi:10.1029/1998GL900117.

Adeniyi, J. O., B. O. Adebesin, I. A. Adimula, O. A. Oladipo, A. O. Olawepo, S. O. Ikubanni, and B. W. Reinisch (2014), Comparison between African equatorial station ground-based inferred vertical E X B drift, Jicamarca direct measured drift, and IRI model, *Adv. Space Res.*, *54*, 1629–1641, doi:10.1016/j.asr.2014.06.014.

Anderson, D., A. Anghel, K. Yumoto, M. Ishitsuka, and E. Kudeki (2002), Estimating daytime vertical ExB drift velocities in the equatorial *F*-region using ground-based magnetometer observations, *Geophys. Res. Lett.*, *29*(12), 1596, doi:10.1029/2001GL014562.

Anderson, D., A. Anghel, J. Chau, and O. Veliz (2004), Daytime vertical E _ B drift velocities inferred from ground based magnetometer observations at low latitudes, *Space Weather*, *2*, S11001, doi:10.1029/2004SW000095.

Bertoni, F., I. S. Batista, M. A. Abdu, B. W. Reinisch, and E. A. Kherani (2006), A comparison of ionospheric vertical drift velocities measured by digisonde and incoherent scatter radar at the magnetic equator, *J. Atmos. Sol. Terr. Phys.*, *68*(6), 669–678, doi:10.1016/j.jastp.2006.01.002.

Bibl, K., and B. W. Reinisch (1978), The universal digital ionosonde, *Radio Sci.*, *13*(3), 519–530, doi:10.1029/RS013i003p00519.

Buonsanto, M. J. (1999), Ionospheric storms—A review, *Space Sci. Rev.*, *88*, 563–601.

Cannon, P. S., B. W. Reinisch, J. Buchau, and T. W. Bullett (1991), Response of the polar cap *F* region convection direction to changes in the interplanetary magnetic field: Digisonde measurements in northern Greenland, *J. Geophys. Res.*, *96*(A2), 1239–1250, doi:10.1029/90JA02128.

Deshpande, M. R., et al. (1977), Effect of electrojet on the TEC of the ionosphere over India subcontinent, *Nature*, *265*, 599–600.

Dunford, E. (1967), The relationship between the ionospheric equatorial anomaly and the *E*-region current system, *J. Atmos. Terr. Phys.*, *29*, 1489–1498.

Grant, I. F., J. W. MacDougall, J. M. Ruohoniemi, W. A. Bristow, G. J. Sofko, J. A. Koehler, D. Danskin, and D. André (1995), Comparison of plasma flow velocities determined by the ionosonde Doppler drift technique, SuperDARN radars, and patch motion, *Radio Sci.*, *30*(5), 1537–1549, doi:10.1029/95RS00831.

Gurney, K. (1997), *An Introduction to Neural Networks*, UCL Press Limited, London.

Ho, C. M., B. D. Wilson, A. J. Mannucci, U. J. Lindqwister, and D. N. Yuan (1997), A comparative study of ionospheric total electron content measurements using global ionospheric maps of GPS, TOPEX radar, and the Bent model, *Radio Sci.*, *32*, 1499–1512, doi:10.1029/97RS00580.

Huang, Y.-N., K. Cheng, and S.-W. Chen (1989), On the equatorial anomaly of the ionospheric total electron content near the Northern Anomaly Crest Region, *J. Geophys. Res.*, *94*, 13,515–13,525, doi:10.1029/JA094iA10p13515.

Huba, J. D., G. Joyce, and J. A. Fedder (2000), Sami2 is Another Model of the Ionosphere (SAMI2): A new low-latitude ionosphere model, *J. Geophys. Res.*, *105*(A10), 23,035–23,053, doi:10.1029/2000JA000035.

Iijima, B. A., I. L. Harris, C. M. Ho, U. J. Lindqwister, A. J. Mannucci, X. Pi, M. J. Reyes, L. C. Sparks, and B. D. Wilson (1999), Automated daily process for global ionospheric total electron content maps and satellite ocean altimeter ionospheric calibration based on Global Positioning System data, *J. Atmos. Sol. Terr. Phys.*, *61*, 1205–1218.

Kil, H., L. J. Paxton, X. Pi, M. R. Hairston, and Y. Zhang (2003), Case study of the 15 July 2000 magnetic storm effects on the ionosphere-driver of the positive ionospheric storm in the winter hemisphere, *J. Geophys. Res.*, *108*(A11), 1391, doi:10.1029/2002JA009782.

Lei, J., J. P. Thayer, J. M. Forbes, Q. Wu, C. She, W. Wan, and W. Wang (2008), Ionosphere response to solar wind high-speed streams, *Geophys. Res. Lett.*, *35*, L19105, doi:10.1029/2008GL035208.

Mannucci, A. J., B. D. Wilson, D. N. Yuan, C. M. Ho, U. J. Lindqwister, and T. F. Runge (1998), A global mapping technique for GPS derived ionospheric total electron content measurements, *Radio Sci.*, *33*, 565–582, doi:10.1029/97RS02707.

McDonald, S. E., C. Coker, K. F. Dymond, D. N. Anderson, and E. A. Araujo Pradere (2011), A study of the strong linear relationship between the equatorial ionization anomaly and the prereversal E × B drift velocity at solar minimum, *Radio Sci.*, *46*, RS6004, doi:10.1029/2011RS004702.

Patra, A. K., P. P. Chaitanya, Y. Otsuka, T. Yokoyama, M. Yamamoto, R. A. Stoneback, and R. A. Heelis (2014), Vertical ExB drifts from radar and C/NOFS observations in the Indian and Indonesian sectors: Consistency of observations and model, *J. Geophys. Res. Space Physics*, *119*, 3777–3788, doi:10.1002/2013JA019732.

Rama Rao, P. V. S., S. Gopi Krishna, K. Niranjan, and D. S. V. V. D. Prasad (2006), Temporal and spatial variations in TEC using simultaneous measurements from the Indian GPS network of receivers during the low solar activity period of 2005–2005, *Ann. Geophys.*, *24*, 3279–3292.

Rastogi, R. G., and J. A. Klobuchar (1990), Ionospheric electron content within the equatorial F_2 layer anomaly belt, *J. Geophys. Res.*, *95*, 19,045–19,052, doi:10.1029/JA095iA11p19045.

Scherliess, L., and B. G. Fejer (1999), Radar and satellite global equatorial *F* region vertical drift model, *J. Geophys. Res.*, *104*(A4), 6829–6842, doi:10.1029/1999JA900025.

Schunk, R. W., et al. (2004), Global Assimilation of Ionospheric Measurements (GAIM), *Radio Sci.*, *39*, RS1S02, doi:10.1029/2002RS002794.

Sivanandam, S. N., and S. N. Deepa (2006), *Introduction to Neural Networks Using Matlab 6.0*, Tata McGraw Hill Comp., New Delhi.

Stolle, C., C. Manoj, H. Lühr, S. Maus, and P. Alken (2008), Estimating the daytime equatorial ionization anomaly strength from electric field proxies, *J. Geophys. Res.*, *113*, A09310, doi:10.1029/2007JA012781.

Stoneback, R. A., R. A. Heelis, A. G. Burrell, W. R. Coley, B. G. Fejer, and E. Pacheco (2011), Observations of quiet time vertical ion drift in the equatorial ionosphere during the solar minimum period of 2009, *J. Geophys. Res.*, *116*, A12327, doi:10.1029/2011JA016712.

Stoneback, R. A., R. L. Davidson, and R. A. Heelis (2012), Ion drift meter calibration and photoemission correction for the C/NOFS satellite, *J. Geophys. Res.*, *117*, A08323, doi:10.1029/2012JA017636.

Su, Y. Z., K.-I. Oyama, G. J. Bailey, T. Takahashi, and S. Watanabe (1995), Comparison of satellite electron density and temperature measurements at low latitudes with a plasmasphere-ionosphere model, *J. Geophys. Res.*, *100*, 14,591–14,605, doi:10.1029/95JA00682.

Uma, G., et al. (2012), Ionospheric responses to two large geomagnetic storms over Japanese and Indian longitude sectors, *JASTP*, *74*, 94–110, doi:10.1016/j.jastp.2011.10.001.

Wan, W., L. Liu, X. Pi, M.-L. Zhang, B. Ning, J. Xiong, and F. Ding (2008), Wavenumber-4 patterns of the total electron content over the low latitude ionosphere, *Geophys. Res. Lett.*, *35*, L12104, doi:10.1029/2008GL033755.

Whalen, J. A. (2004), Linear dependence of the postsunset equatorial anomaly electron density on solar flux and its relation to the maximum prereversal E × B drift velocity through its dependence on solar flux, *J. Geophys. Res.*, *109*, A07309, doi:10.1029/2004JA010528.

Woodman, R. F., J. L. Chau, and R. R. Ilma (2006), Comparison of ionosonde and incoherent scatter drift measurements at the magnetic equator, *Geophys. Res. Lett.*, *33*, L01103, doi:10.1029/2005GL023692.

Yue, X., W. Wan, J. Lei, and L. Liu (2008), Modeling the relationship between EXB vertical drift and the time rate of change of h_mF_2 ($\Delta h_mF_2/\Delta t$) over the magnetic equator, *Geophys. Res. Lett.*, *35*, L05104, doi:10.1029/2007GL033051.

Zhao, B., W. Wan, L. Liu, and T. Mao (2007), Morphology in the total electron content under geomagnetic disturbed conditions: Results from global ionosphere maps, *Ann. Geophys.*, *25*, 1555–1568.